

Current Capabilities of the Residual Stress Diffractometer at the High Flux Isotope Reactor

P. Cornwell,¹ J. Bunn,¹ C.M. Fancher,¹ E.A. Payzant¹, C.R Hubbard²

¹*Neutron Scattering Science Division, Oak Ridge National Laboratory, Oak Ridge, Tennessee, 37830, USA*

²*Material Science and Technology Division, Oak Ridge National Laboratory, Oak Ridge, Tennessee, 37830, USA (Retired)*

This manuscript has been authored by UT-Battelle, LLC under Contract No. DE-AC05-00OR22725 with the U.S. Department of Energy. The United States Government retains and the publisher, by accepting the article for publication, acknowledges that the United States Government retains a non-exclusive, paid-up, irrevocable, worldwide license to publish or reproduce the published form of this manuscript, or allow others to do so, for United States Government purposes. The Department of Energy will provide public access to these results of federally sponsored research in accordance with the DOE Public Access Plan (<http://energy.gov/downloads/doe-public-access-plan>).

The engineering diffractometer Neutron Residual Stress Facility (NRSF2) at Oak Ridge National Laboratory's High Flux Isotope Reactor (HFIR) was built specifically for the mapping of residual strains. NRSF2 is optimized to investigate a wide range of engineering materials by providing the user a selection of monochromatic neutron wavelengths to maintain the selected Bragg reflection near $2\theta = 90^\circ$, which is the optimal scattering geometry for strain mapping. Details of the instrument configuration and operation are presented and considerations for experimental planning are also discussed. Selected examples of recent residual stress work completed at NRSF2 are presented to highlight capabilities.

I. INTRODUCTION:

The 2nd Generation Neutron Residual Stress Facility (NRSF2) is a high-flux engineering diffractometer ideal for spatial characterization of residual stress in large-scale engineering components and is located at the High Flux Isotope Reactor (HFIR) at Oak Ridge National Laboratory (ORNL). NRSF2 was designed with flexibility in mind, meaning the instrument can be readily reconfigured to fit the needs defined by the geometry of the material of interest. The high penetrating power of thermal neutrons enables in-depth bulk measurement of residual stress which is ideal for non-destructive inspection. NRSF2 exploits the ability to perform bulk measurements at various depths in materials to acquire a more complete picture of residual stresses and their gradients in the engineering component.

Unlike a typical powder diffractometer, the key feature of an engineering diffractometer is that the geometry of the sample defines the instrument configuration. A few grams of powder in a sealed can is optimal for crystal structure determination, whereas engineering instruments characterize large-scale microstructural effects in comparatively large samples. For the case of strain mapping, the spatial resolution is defined by a gauge volume, governed by incident and diffracted slits, within a large sample, as shown in FIG. 1. The sample may be translated and rotated with respect to the gauge volume, thereby enabling mapping of directionally dependent strains in the sample [1].

The mapping capabilities of NRSF2 are achieved through careful selection of suitable sample positioners, multi-wavelength monochromator, detector array, variable gauge volume, data collection and analysis software, and optical alignment system, as will be discussed. The NRSF2 sample goniometer can manipulate samples up to 2400 kg. – dependent upon the configuration. The multi-wavelength monochromator provides six discrete individually selectable wavelengths ranging from 1.45-2.67Å, with the highest flux on sample (3×10^7 n/cm²/s) for either the Si 331 or Si 400 monochromator reflections. This ability to select wavelength is essential in a reactor instrument, since the best mapping results are obtained when the diffraction peak of interest is located near $2\theta = 90^\circ$, thereby preserving a reasonably rectilinear gauge volume. The monochromator has direct line-of-sight to the reactor core via a thermal beam tube. The detector system currently consists of seven ORDELA linear position sensitive detectors in a vertical array with a range of $4^\circ 2\theta$. Gauge volume linear dimensions range from 0.3mm - 20mm depending on slit configuration [1].

NRSF2 has its origins in a 1992 Laboratory Directed R&D (LDRD) project by Cam Hubbard, Steve Spooner, and Stan David, which lead to a “residual stress” instrument, NRSF, funded through the former High Temperature Materials Lab (HTML) user program, and which from 1994-2001 shared time on the former HB-2 triple axis spectrometer [2]. The success of the growing user community eventually led to construction of a dedicated residual stress mapping instrument, NRSF2, first online in 2004. Following the conclusion of the HTML user program, it was decided that the neutron sciences user program would manage this instrument, which saw a series of software and hardware upgrades.

NRSF2 is not the only reactor-based engineering diffractometer idealized for strain scanning currently operating in the world. Other instrument include the BT8 Residual Stress Diffractometer at the National Institute of Standards and Technology (NIST) located in Gaithersburg, Maryland in the United States [3], KOWARI at the Australian Nuclear Science and Technology Organization (ANSTO) in New South Wales, Australia [4], STRESS-SPEC at the Hein Maier-Leibnitz Zentrum (MLZ) located in

Munich, Germany [5], and the ST-1 instrument at the Korean Atomic Energy Research Institute (KAERI) located in Daejeon, South Korea [6].

II. INSTRUMENTATION AND DESIGN:

1. Monochromator:

NRSF2 uses double-bent (vertical and horizontal) monochromators,[7, 8] which provide a high flux. The monochromator assembly features two back-to-back stacked silicon wafer-based monochromators (220 and 511 cuts) separated by a borated aluminum plate to mitigate unwanted signal from the opposing stack. The Si wafers are at a fixed, vertically bent angle while the horizontal direction can be “focused,” in combination with a motorized tilt axis to optimize the flux on the sample. Varying the monochromator orientation with respect to the take-off angle allows the selection from seven reflections (Table 1) with wavelengths optimized for measurement of typical engineering alloys (*e.g.*, Fe, Al, Ni, and Cu).

TABLE I. List of monochromatic reflections with associated wavelengths for an 88° fixed takeoff angle. The relative intensities are taken from the upstream monitor.

Reflection	Wavelength [Å]	Relative Intensity, [arb]
Si 333	1.452Å	1600
Si 511	1.452Å	700
Si 422	1.540Å	1600
Si 331	1.731Å	1800
Si 400	1.886Å	1200
Si 311	2.275Å	650
Si 220	2.667Å	900

2. Optics:

The incident and diffracted beams are defined using gadolinium slits with selected dimensions between 0.3 – 20mm. Slits are mounted in boron carbide (B₄C) composite housings which provide complete shielding of the monochromatic neutron flux. The use of a B₄C housing shields the detector from stray neutrons originating from unwanted regions of interest in the sample. This housing reduces the overall

measured background signal from errant environmental sources. Each slit system mounts on an optical rail which is aligned prior to measurements. The incident slit assembly is precisely adjusted to position the incident beam over the goniometer center of rotation, and the diffracted beam slit assembly is adjusted to orient the detector field of view over the same center of rotation. FIG. 2 shows a schematic representation of the optic system utilized at NRFS2.

3. Motion controls and sample positioning:

The goniometer uses a multi-axes system for sample manipulation such that user specified locations and direction may be investigated. All motors/axes are controlled using a Galil 4080 multi-axis controller. The axes and their respective reproducibility detailed in TABLE II. The higher precision of the 2θ axes is a consequence of the Heidenhain encoder which is required to meet the precision requirements of residual stress mapping. The fixed beam height lies approximately 390 mm above the X-Y translation stage. This fixed height imposes the largest limiting factor in strain mapping.

TABLE II. Instrument positioning system specifications

Axis Name	Range	Motion Type	Reproducibility
SX	$\pm 190\text{mm}$	Linear	0.05mm
SY	$\pm 90\text{mm}$	Linear	0.05mm
Omega	279°	Rotation	0.05°
2Theta	$70^\circ\text{-}115^\circ$	Rotation	0.003°
EZ-elevator	250mm	Linear	0.05mm
Z-translation	340mm	Linear	0.05mm
SZS	88mm	Linear	Varies up to 0.05mm
Phi	360°	Rotation	0.05
Chi	360°	Rotation	0.05

4. Detector configuration:

NRSF2 uses a 7-detector vertical array comprised of linear position sensitive ^3He detectors (ORDELA model 1155N) with 1 detector in the scattering plane, and 6 detectors offset evenly above or below the horizontal plane (excluding the horizontal detector) by increments of $\sim\pm 5.6^\circ$ for a total span of 33.6° (defined from detector centers). The configuration of the detector array is shown in FIG. 3. The ORDELA

1155N detectors have an active area of 90 mm by 40 mm. A multichannel analyzer is used to collect and bin the detector output signals into 528 channels per detector. The detector system is shielded using ${}^6\text{Li}$ and steel-polymer sheets to mitigate the detection of stray neutrons.

5. Instrument alignment and calibration:

Precise calibration and alignment of the instrument and alignment of the sample is critical for mapping residual stresses. The instrument optics are first aligned to a precision of +/- 50 micron. Aligning the optics ensures that the gauge volume does not precess during sample manipulation.

The instrument is calibrated to ensure proper reduction of raw data using the following process. Incoherent scattering from a Vanadium pin is used to correct for the counting efficiency of each individual channel in all seven detectors. The width of the detector channels in each detector is determined by stepping the detector over a known diffraction peak and utilizing the precision of the Heidenhain encoder to know the 2θ value. Powder standards (Fe, Ge, Ca, Mo, Ni) are measured to quantify the 2θ offset and out-of-plane position of each detector to account for the Debye cone effect induced peak shift. Statistical analysis of calibration data suggest that the highest achievable strain resolution is ~50 microstrain.[9]

Precise sample alignment allows for the placement of the gauge volume at known positions within a sample. An initial rough alignment is performed an optical theodolite, then refined by the measurement of neutron intensity scans. These alignments can be complex and time consuming; however, are critical to ensure proper interpretation of strain mapping results.

6. Data acquisition and analysis:

The data acquisition and analysis software have been built using the National Instrument LabVIEW™ framework. A modified version of the data acquisition software, Spectrometer Instrument Control Environment (SpICE Residual Stress 1.6.6.26), is used to control the instrument and acquire data through the running or scripts or user defined macros.[10] Raw diffraction data are corrected and reduced using the NRSF2 View (v.3.0.2).[11]

III. APPLICATIONS:

NRSF2 is used for strain mapping of welds (thermal and friction stir), heat-treated samples, forgings, extrusions, bearings and races, fasteners, components for transportation and aerospace, pressure vessels and piping, nuclear engineering components, and parts made through additive manufacturing. Neutron diffraction studies of materials under applied stress reveal phase- and grain-level knowledge of

deformation processes, which are fundamental for developing finite-element and self-consistent field models of materials behavior. More complex experiments have included functional materials; such as piezoelectric materials in applied fields, and shape-memory alloys under varying load and temperature conditions.[12, 13] Additional examples of recent experiments are highlighted below.

1. Mapping and modeling of residual stresses across a dissimilar weld:

The stress distributions from dissimilar metal (ferritic-austenitic) welds are asymmetric due to phase transformation and the different materials properties. Neutron diffraction was utilized to map the stress distribution in the complex behaving welds (FIG. 4). The study of residual stress distributions in dissimilar welds in this study provides new insights into the magnitude of the stresses resulting from joining metals with different structures and physical properties.[14] Typical heat treatment processes cannot be used to relieve the residual stresses due to the difference in thermal expansion coefficients of the different metals. This data has been used to verify finite element models being developed by Clarkson University.[15]

2. Mapping stresses in a tubular weld joint after fatigue cycling:

Stress distributions resultant from welded tubular joints were mapped for two different structural steels before and after fatigue. A pearlitic-ferritic (bcc) steel joint, as well as an austenitic (fcc) steel were investigated (FIG. 5). In addition, the weld was measured before and after a specialized fatigue test was performed. These measurements of the residual stress evolution in the samples is important for lifetime expectation of the welds in service. Phase transformations which occur in the S355JH+N steel were found to have a marked effect on stress distribution. This work provides new insights into the nature and magnitude of the stresses resulting from joining metals in a tubular joints which have undergone very few fatigue cycles after welding[16, 17].

3. Mapping residual stress distributions in a complex AM part for use in NASA rockets:

The NASA Marshall Space Flight Center (MSFC) has initiated the development of additive manufacturing (AM) for both on-earth and, more importantly, in-space applications. AM is an attractive manufacturing route because AM can enable on-demand production of parts, tools, or structures of complex space-flight hardware. Selective Laser Melting (SLM) is an on-earth AM technology that MSFC is using to build Alloy 718 rocket engine components. Understanding the SLM-718 material properties is

required to design, build, and qualify components for space flight. Residual stresses are of interest for this AM process, since SLM is a series of ~ 100 μm -wide welds; where highly non-linear heating and cooling, severe thermal gradients and repeated thermal cycling can result in high stress concentrations that may cause degraded material properties, and warp or distort the geometry of SLM components. The residual strain distributions were measured and are shown in FIG. 6. These distortions can render the component out-of-tolerance, and even interrupt or halt the build process if the warped material prevents the SLM machine from operating properly. Severely warped components must be scrapped and re-designed, which is both time consuming and costly. If residual strains are better understood, and can be predicted, these effects can be mitigated in the component's design.[18]

4. Mapping of residual stresses in Stryker vehicle armor plates:

One persistent issue in welding high-strength steels is hydrogen induced cracking (HIC) which is the process where the steel becomes brittle due to the introduction of hydrogen during the welding process. Three essential conditions must co-exist for HIC to occur: the presence/absorption of hydrogen from the welding process or the environment, sensitive hardened microstructure, and high tensile residual stresses (LA-100,

FIG. 7 top). If any one of these conditions are eliminated the occurrence of HIC is reduced. One common method employed to reduce the occurrence of HIC is to preheat the weld prior to welding. This drives off any hydrogen, but also adds time and cost to the welding process. For military applications, the ideal condition is to weld without preheating, thus a different approach is needed to mitigate hydrogen induced cracking. This study has taken an entirely different approach to the mitigation of HIC. The team has developed a weld wire chemistry (LTT wire HV1766,

FIG. 7 bottom) that does not require preheating. The weld wire changes the stress state, *in situ*, at the weld site through a martensitic phase transformation to martensite; which reduces the tensile stress and in most cases, changes the stress state from tensile to compression[19].

III. Experimental Planning Considerations:

Multiple factors must be considered when planning a residual stress experiment.

- 1) A well-known reference lattice spacing (d_0) is needed.
- 2) Ideally the diffracted slit should be placed as close as possible to the sample to reduce broadening of the gauge volume by the pinhole effect.

- 3) The time required to measure statistically significant data is dependent on the size of the gauge volume and the magnitude of beam attenuation (signal loss), which depends upon material microstructure and path length of incident/diffracted beam into and out of the sample. For example, a larger gauge volume facilitates quick measurement and deeply buried gauge volumes will require longer counting times.
 - a. Also, as the gauge volume increases the divergence of the beam will increase at a similar ratio. More importantly the distance between the incident and diffracted slit assemblies must be minimized to more accurately determine a gauge volume size.
- 4) Care must be taken to ensure that the gauge volume is always buried to prevent anomalous shifts associated with partially buried gauge volume effect that has been well documented by Spooner, *et al.*[20] as to cause artificial peak shifts leading to misrepresentation of the strain values.
- 5) For the calculation of stress, a minimum of three orthogonal directions of strain must be measured. If the strain directions are not along the principal axes, additional measurements are required for the stress tensor calculation.
- 6) The residual stress technique requires many grains contributing to diffraction in the measured gauge volume. Microstructural effects including grain size and texture need to be considered. Large grains with respect to the gauge can lead to poor counting statistics, anomalous peak shifts and spotty diffraction rings. Texture in a sample can increase collection times do to the need to oscillate the rotation of the sample for grain averaging.
- 7) Chemistry variations can lead to spatial changes in d_0 of the material, resulting in anomalous strains. This is significant for the measurement of strains in welding heat-affected-zones, rapidly solidified and/or carburized materials.

IV. FUTURE INSTRUMENT UPGRADES:

NRSF2 is currently in the processes of upgrading essential instrument components. The array of 7 detectors will be replaced by a single two-dimensional PSD (DENEX 300TN) which has a larger 2θ field of view both in- and out-of-plane. A two-dimensional PSD is expected to bring a significant improvement in capabilities and will require changes in how NRSF2 is configured and operated (*e.g.*, optics, DAQ, and data analysis). NRSF2's diffraction slit optic solution will be augmented by an interchangeable radial collimator, while the incident optics will be replaced by a fully automated solution (JJ-Xray model IB-C30-AIR). The diffracted optics will leverage AM capabilities to enable custom-built low-cost polymeric radial collimators.

ACKNOWLEDGMENTS:

The authors thank the effort of past and present team members and users for their countless contributions. In particular, the authors thank Alexandru Stoica, Stan David, and Steven Spooner for their contributions to the initial instrument design, Barton Bailey for his engineering effort in designing the current instrument, Steve Kulan, Ray Gregory, and Larry Senesac, and Brian Cady for their effort on DAS and Ron Maples for his work on the DAQ system. This research used resources at the High Flux Isotope Reactor, a DOE Office of Science User Facility operated by the Oak Ridge National Laboratory.

REFERENCES:

1. Hutchings, M.T., et al., *Introduction to the characterization of residual stress by neutron diffraction*. 2005: CRC Press.
2. Spooner, S., et al., *Engineering applications of neutron scattering at the high flux isotope reactor*. Neutron News, 1999. **10**(2): p. 26-30.
3. Brand, P.C., H.J. Prask, and T. Gnaeupel-Herold, *Residual stress measurements at the NIST reactor*. Physica B, 1997. **241**: p. 1244-1245.
4. Kirstein, O., et al., *Kowari – OPAL’s Residual-Stress Diffractometer and its Application to Materials Science and Engineering*. Advanced Materials Research, 2008. **41-42**: p. 439-444.
5. Hofmann, M., et al., *The new materials science diffractometer STRESS-SPEC at FRM-II*. Physica B: Condensed Matter, 2006. **385-386**: p. 1035-1037.
6. Moon, M.-K., et al., *Present status of residual stress instrument at the HANARO*. Physica B: Condensed Matter, 2006. **385-386**: p. 1038-1039.
7. Popovici, M., et al. *Multiwafer focusing neutron monochromators and applications*. in *International Symposium on Optical Science and Technology*. 2001. SPIE.
8. Popovici, M. and W.B. Yelon, *A High Performance Focusing Silicon Monochromator*. Journal of Neutron Research, 1997. **5**(4): p. 227-239.
9. Bunn, J., et al., *Experimental determination of instrumental strain resolution of a neutron engineering diffractometer using thermal expansion*. (Manuscript in preparation).
10. Lumsden, M.D., J.L. Robertson, and M. Yethiraj, *SPICE—Spectrometer and Instrument Control Environment*. Physica B: Condensed Matter, 2006. **385-386**: p. 1336-1339.
11. An, K. and C. Hubbard, *User Manual of the NRSF2-VIEW and NRSF2-CALIBRATE*. 2006.
12. Pramanick, A., et al., *In situ neutron diffraction studies of a commercial, soft lead zirconate titanate ceramic: response to electric fields and mechanical stress*. Applied Physics A, 2010. **99**(3): p. 557-564.
13. Nicholson, D.E., *Multi-axial Thermomechanical Characterization of Shape Memory Alloys for Improved Stability*. 2017, University of Central Florida.
14. Eisazadeh, H., et al., *A Residual Stress Study in Similar and Dissimilar Welds*. Welding Journal, 2016. **95**(4): p. 111S-119S.
15. Eisazadeh, H., J.R. Bunn, and D.K. Aidun, *Numerical and neutron diffraction measurement of residual stress distribution in dissimilar weld*. Welding Journal, 2017. **96**(1).
16. Hempel, N., et al., *Residual Stress Analysis in Girth-welded Ferritic and Austenitic Steel Pipes Using Neutron and X-Ray Diffraction*, in *Residual Stresses 2016: ICRS-10*. 2017. p. 229-234.

17. Hempel, N., et al., *Study on the residual stress relaxation in girth-welded steel pipes under bending load using diffraction methods*. Materials Science and Engineering a-Structural Materials Properties Microstructure and Processing, 2017. **688**: p. 289-300.
18. Bagg, S., L.M. Sochalski-Kolbus, and J. Bunn, *The Effect of Laser Scan Strategy on Distortion and Residual Stresses of Arches Made With Selective Laser Melting*. 2016, NASA: NASA Technical Reports Server. p. 6.
19. Xinghua, Y., et al., *Tensile Residual Stress Mitigation Using Low Temperature Phase Transformation Filler Wire in Welded Armor Plates*, in *Residual Stresses 2016: ICRS-10*. 2017. p. 461-466.
20. Spooner, S. and X.-L. Wang, *Diffraction Peak Displacement in Residual Stress Samples Due to Partial Burial of the Sampling Volume*. Journal of Applied Crystallography, 1997. **30**(4): p. 449-455.

FIGURES:

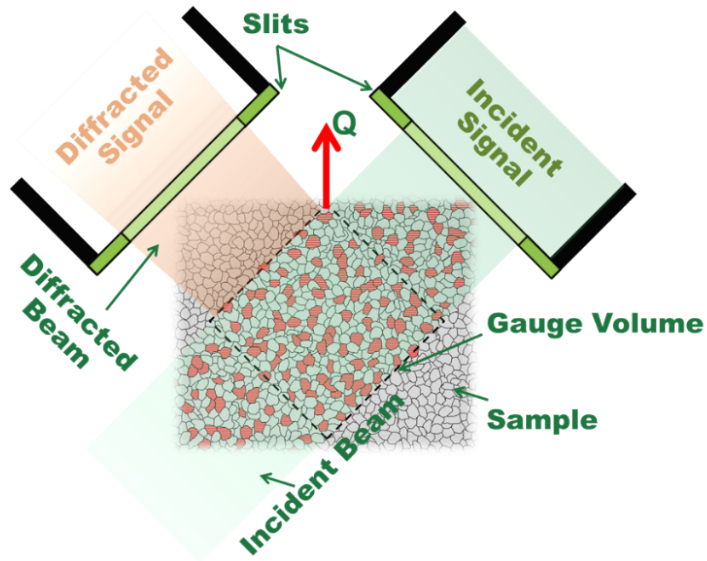


FIG. 1. Sketch detailing the use of slits to define a subset of grains within larger components typical in engineering diffraction mapping experiments. The scattering vector (Q) is shown as a reference to highlight what strain direction is probed, which corresponds to the direction of strain being measured.

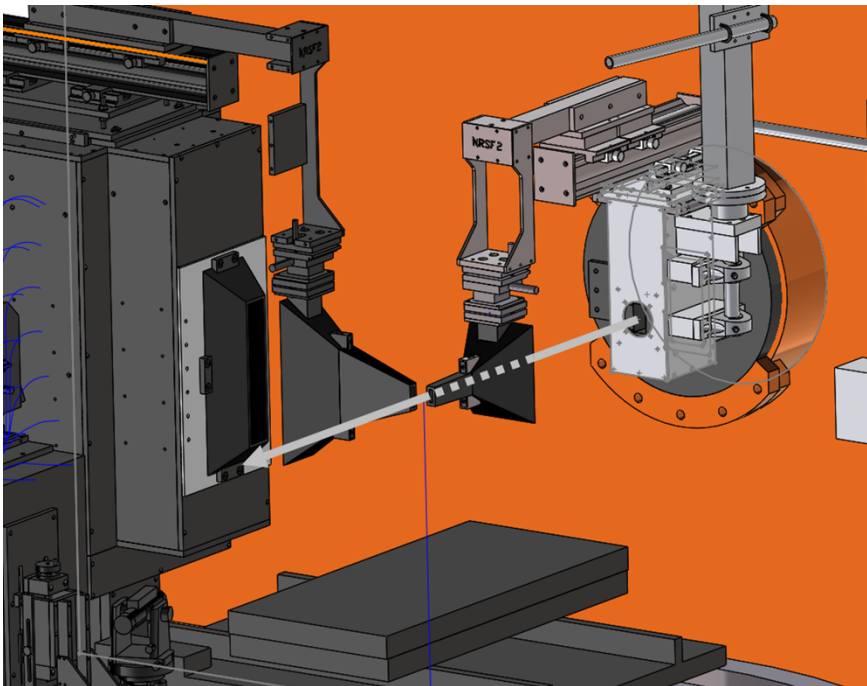


FIG. 2. Side view of the NRSF2 layout illustrating the position of the incident and diffracted snouts that house the slits that define the gauge volume.

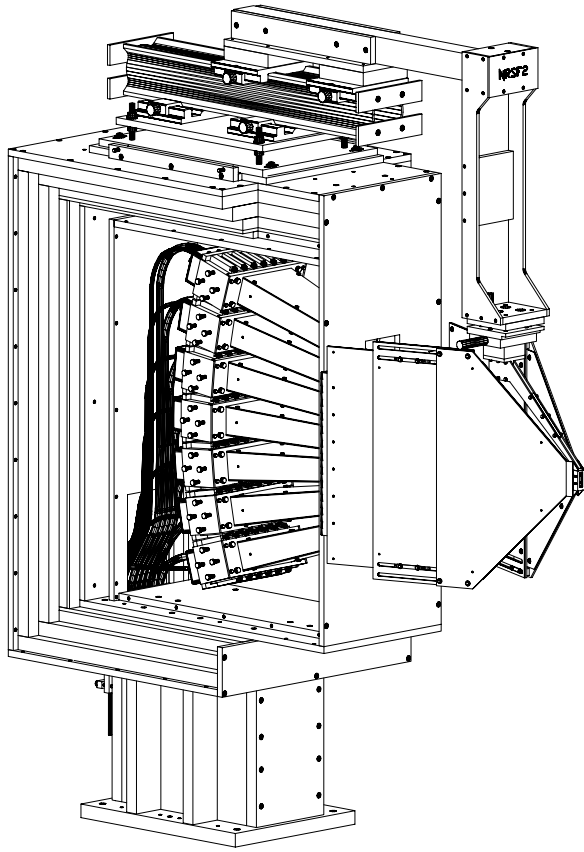


FIG. 3. Side view of the detector box with the array of 7-detectors.

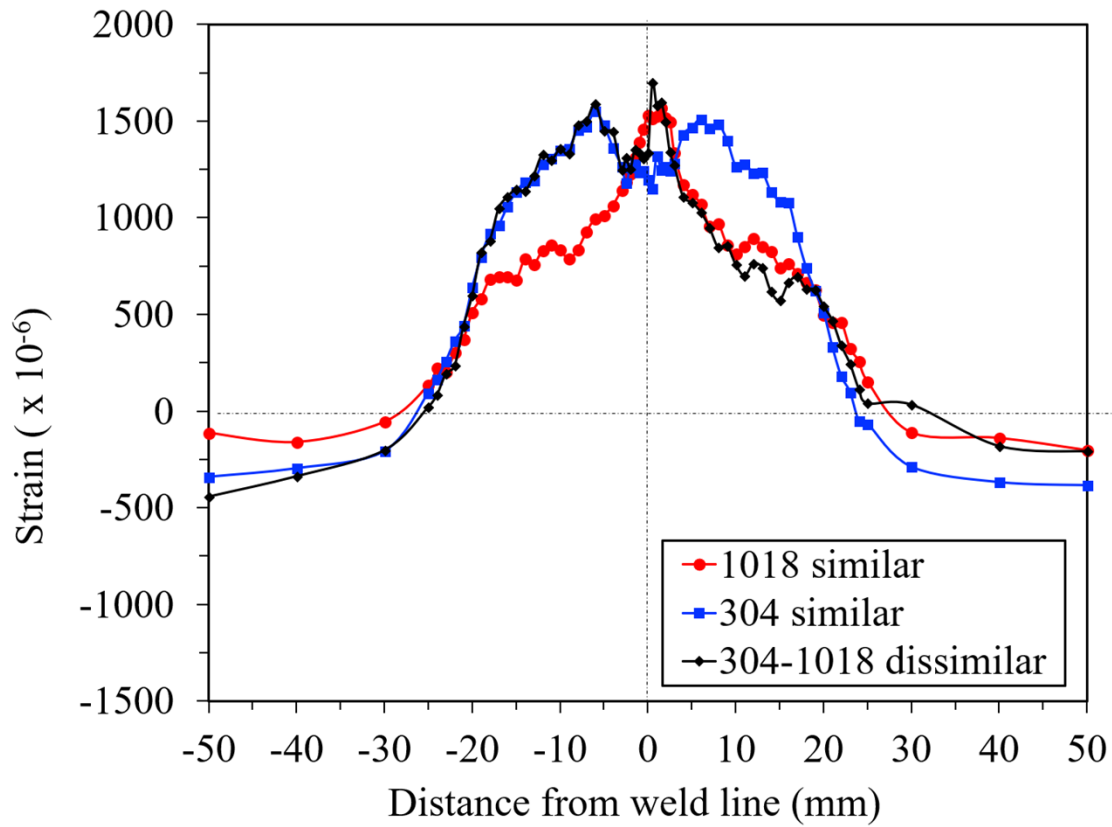


FIG. 4. Distribution of longitudinal strain in 1018 similar, 304 similar, and 304-1018 dissimilar weld.

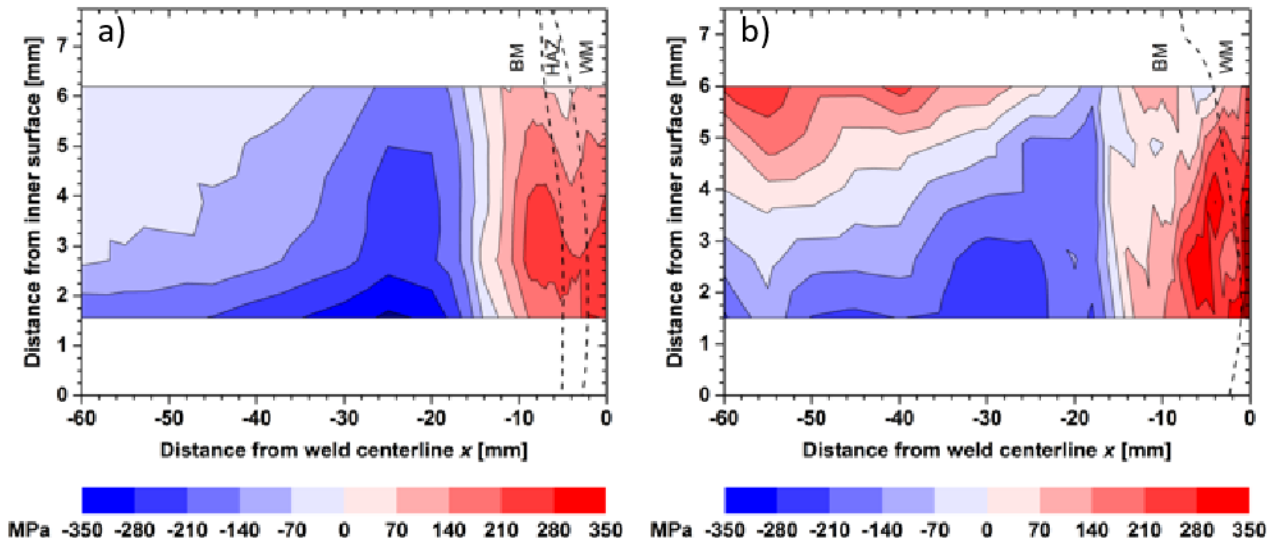


FIG. 5. Hoop residual stress distribution in the pipe wall for a) structural steel S355J2H+N and b) austenitic steel b) X6CrNiTi18-10 measured using ND. Dashed lines represent boundaries between different zones of the weld. Figure adapted with permission from Hempel, N., et al. (2017). Residual

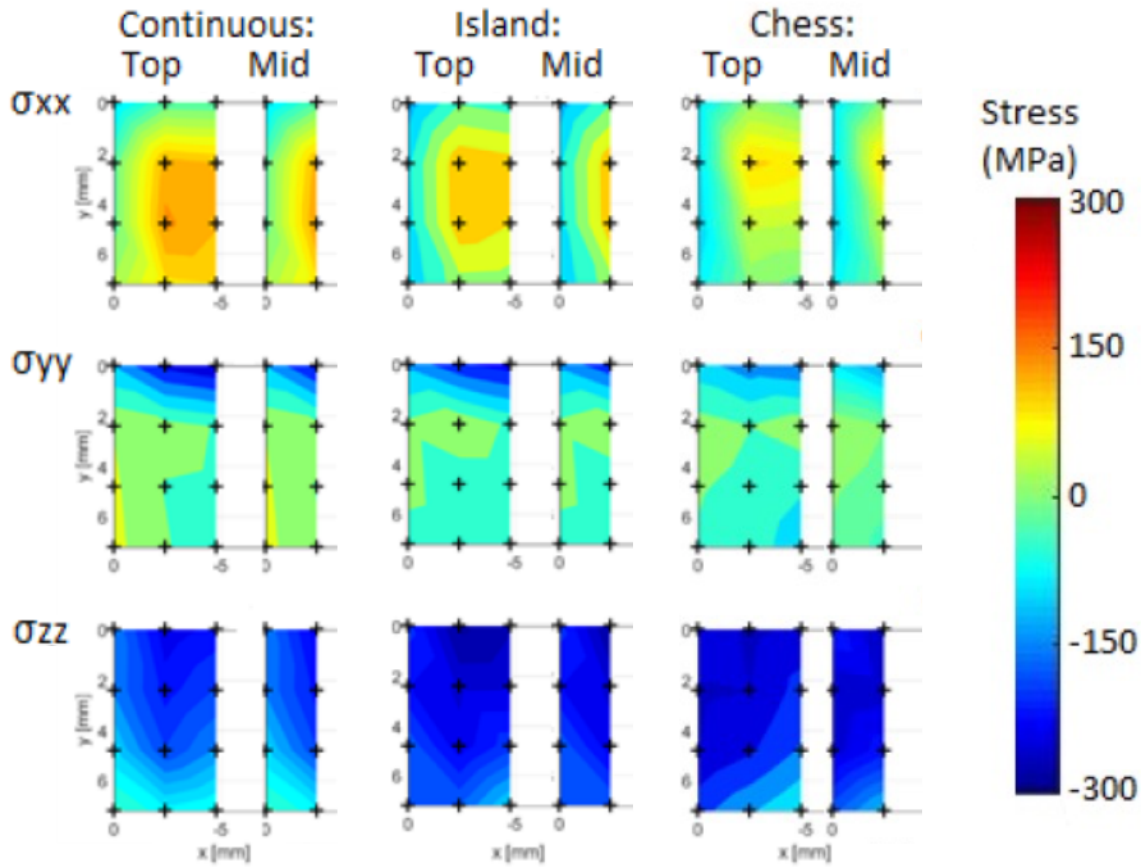


FIG. 6. Comparison of the effect of AM build scan strategies (continuous, island, or chess) on the residual stresses present in Arches that are confined to the build plate. Reproduced with permissions from Bagg, S., et al. (2016). The Effect of Laser Scan Strategy on Distortion and Residual Stresses of Arches Made With Selective Laser Melting. NASA Technical Reports Server, NASA: 6. Document ID: 20160008858

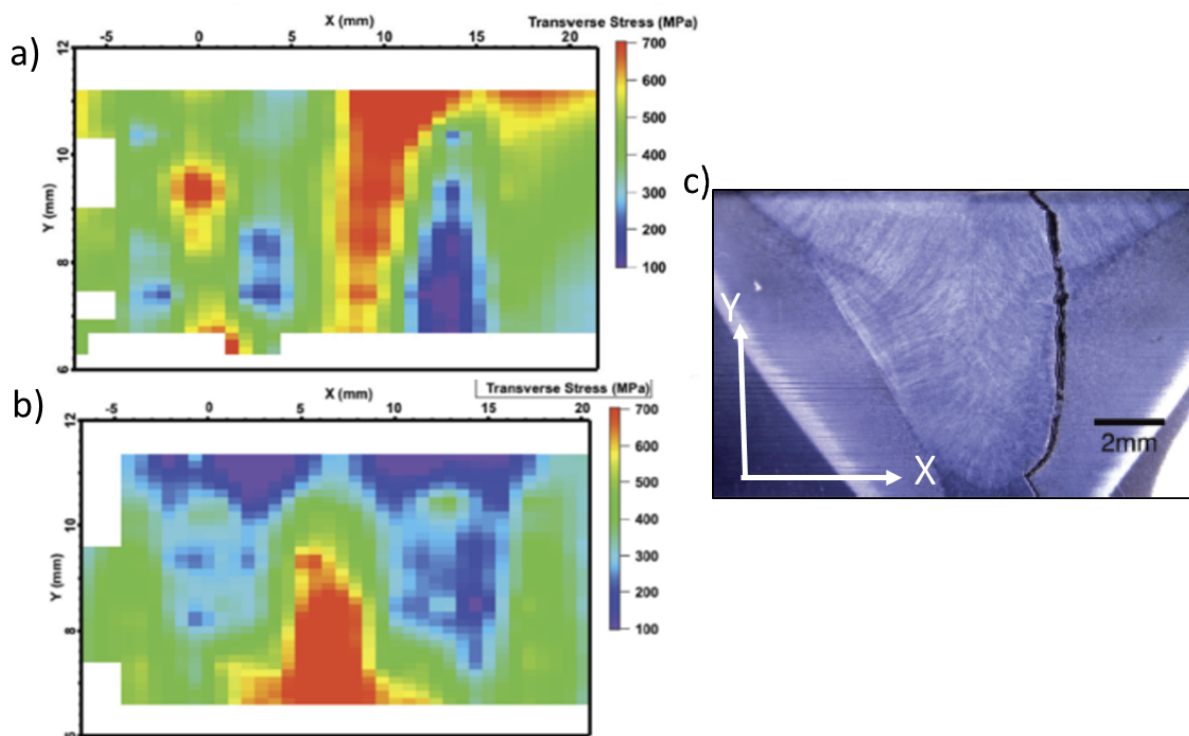


FIG. 7. Longitudinal residual stress distribution of Y-groove plate welded using **a)** LA-100 (typical weld filler wire) (top) and **b)** LTT filler wire HV1766 (bottom). The micrograph in **c)** demonstrates the cracking observed in the LA-100 conventional wire due to the large tensile transverse stress. Figure adapted with permission from Xinghua, Y., et al. (2017). Tensile Residual Stress Mitigation Using Low Temperature Phase Transformation Filler Wire in Welded Armor Plates. Residual Stresses 2016: ICRS-10. 2: 461-466. DOI : 10.21741/9781945291173-78